



ACADÉMIE
DES SCIENCES
INSTITUT DE FRANCE

Comptes Rendus

Physique


Jean-Pierre Gauthier, Thanh Nhan Bui and Jacques Fereire

The cat's-eye phenomenon: a mathematical approach

Volume 26 (2025), p. 181-198

Online since: 6 February 2025

<https://doi.org/10.5802/crphys.231>

 This article is licensed under the
CREATIVE COMMONS ATTRIBUTION 4.0 INTERNATIONAL LICENSE.
<http://creativecommons.org/licenses/by/4.0/>



*The Comptes Rendus. Physique are a member of the
Mersenne Center for open scientific publishing*
www.centre-mersenne.org — e-ISSN : 1878-1535



Research article / *Article de recherche*

The cat's-eye phenomenon: a mathematical approach

L'effet œil-de-chat : une approche mathématique

Jean-Pierre Gauthier ^{*,a}, Thanh Nhan Bui ^b and Jacques Fereire ^a

^a Centre de Recherches Gemmologiques, 2 rue de la Houssinière, 44322 Nantes, France

^b Rue du Compas 47/4, 1070 Bruxelles, Belgium

E-mails: jpk.gauthier@gmail.com (J.-P. Gauthier), tnhan93@gmail.com (T. N. Bui), jacques.fereire@hotmail.fr (J. Fereire)

Abstract. This paper provides a mathematical basis for the well-known cat's-eye effect appearing on chatoyant gemstones. After reminding the reader of the physical origin of this effect and the conditions for observing it, we introduce all required parameters and some reasonable assumptions in order to simplify the calculations. In fact, we describe the motion of a point located at the apex of the cat's-eye line in the "main" plane, defined by the directions of the source and the observer and perpendicular to the set of acicular inclusions responsible for the optical phenomenon. These calculations confirm the qualitative cat's-eye behavior commonly observed in various situations, when the source or the observer moves around the cabochon or when the stone rotates under them.

Résumé. Le but de cet article est de donner une base mathématique à l'effet bien connu d'œil-de-chat apparaissant sur les pierres précieuses chatoyantes. Après avoir rappelé l'origine physique de cet effet et les conditions de son observation, nous introduisons tous les paramètres nécessaires à cette étude et quelques hypothèses raisonnables afin de simplifier les calculs. En fait, nous décrivons le mouvement d'un point situé à l'apex de la ligne de l'œil-de-chat dans le plan "principal", défini par les directions de la source et de l'observateur et perpendiculaire à l'ensemble des inclusions aciculaires responsables du phénomène optique. Ces calculs confirment le comportement qualitatif de l'œil-de-chat couramment observé dans diverses situations, lorsque la source ou l'observateur se déplacent autour du cabochon ou lorsque la pierre tourne sous eux.

Keywords. Chatoyancy, Cat's-eye, Asterism, Optical phenomenon, Mathematical approach.

Mots-clés. Chatoyance, Œil-de-chat, Astérisme, Phénomène optique, Approche mathématique.

Manuscript received 9 May 2024, revised 27 October 2024 and 27 December 2024, accepted 30 December 2024.

1. Introduction

Numerous minerals exhibit chatoyancy or asterism. Chatoyancy is an optical phenomenon that creates a band of light moving across a material's surface (or several bands in the case of asterism). The book by Steinbach [1] gives a comprehensive account of the most well-known, spectacular and common to the rarest of these gems showing these particular effects, and lists over 200

*Corresponding author

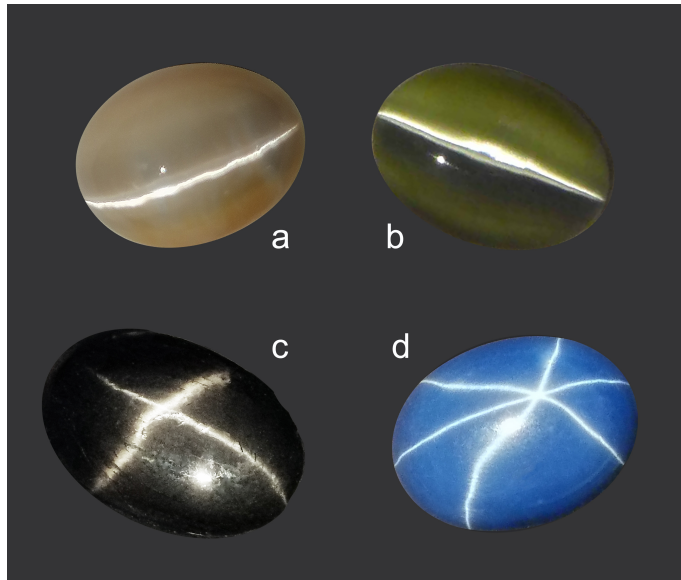


Figure 1. Chatoyancy caused by (a) hollow tubes in a Tanzanian cat's-eye opal (2.95 cts); (b) optical fibers in an imitation cat's-eye (4.56 cts); (c) magnetite needles in a 4-ray star diopside (21.70 cts); (d) rutile needles in a 6-ray synthetic star sapphire (10.75 cts). Photos: J. P. Gauthier.

mineral species chatoyant or asteriated. Cat's-eyes and stars that can be observed on gems cut *en cabochon* (gem with a curved surface instead of faceted) are basically mobile depending on different parameters, such as the position of the source or the observer and the stone orientation. If the physical origin of this optical phenomenon is well known, its mathematical description has never been achieved. We propose to follow the path of a light ray at the origin of the phenomenon in some particular cases and to carry out a mathematical study for these various parameters. For clarity, each case considered will be followed by a short conclusion, in bold.

2. The cat's-eye phenomenon: physical bases

The cat's-eye effect has long been physically described in various papers [2–5]. It arises from the light scattering on acicular (needle-like) structures, whether they are exsolutions or tubular cavities present in a single-crystal mineral matrix or even fibrous materials (Figure 1). From now on, for simplicity, we will use the term “needles” to refer to tubes, needles, and fibers.

A 3D simulation of the phenomenon was proposed by Yokoi et al. [6] using a model of needles with microfacets, for which these authors developed an algorithm to describe the distribution of rays scattered by the inclusions. However, the purpose of this work was to build a model illustrating the movement of the cat's-eye or the star during the rotation of the stone, not to mathematically explain the phenomenon.

The physical basis of light scattering is quite simple to describe when a single ray of light falls on a thin isolated needle placed in air. However, the optical effect known as chatoyancy, which results from the refraction of a light beam on a cabochon followed by scattering on a set of parallel needles grown along a particular direction within a mineral matrix (exsolved inclusions) is more challenging to study in a comprehensive way. We will therefore gradually analyze different aspects of this “cat's-eye” effect.

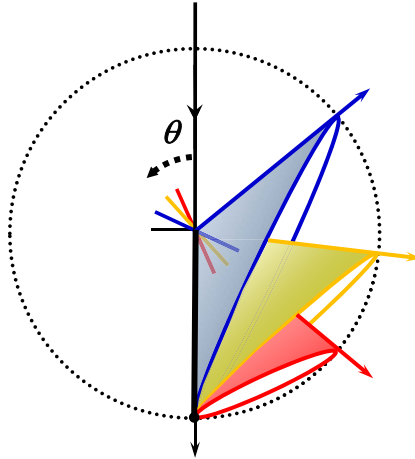


Figure 2. A needle placed in the air forming different angles θ with respect to the incident ray scatters the light into hollow conical veils. The needle being placed at the center of a virtual sphere, the scattering cones intercept it in circular rings, which all share a common point at the lower pole, and widen in diameter as the needle moves away from the vertical. Two particular cases may be emphasized: (i) when the needle is vertical, the scattering cone is reduced to a line emerging at the lower pole; (ii) when the needle is horizontal, the cone becomes flat (vertical disc).

3. Scattering of a light beam by a thin needle in the air

The theory developed by the authors referred to in the previous paragraph tells us that when a light beam hits a very thin linear scatterer, it is scattered as a conical surface of light centered on the long axis of the needle, and having as half top angle (i.e. angle generating a cone by rotation around an axis) the angle θ between the incident beam and the needle (Figure 2). Therefore, regardless of the direction of the needle, i.e. regardless of the opening of the cone angle, the incident ray is always one of the lines generating the cone. As the needle tilt increases relative to the vertical beam, the scattering cone gradually opens, until the cone becomes flat when the needle is perpendicular to the incident ray.

To visualize this effect, one can imagine the incident beam entering through a hole drilled in a translucent sphere acting as a screen. At the center of the sphere lies a needle that moves in various directions. The hollow cones of scattered light will then cross the screen as luminous circles.

4. Scattering of a light beam by parallel needles exsolved in a mineral with a flat or curved surface

The scattering phenomenon should now be applied not to a single needle in air, but to a set of parallel needles embedded into a single crystal. A ray of light hitting the surface is first refracted, then scattered by the needles and again refracted out of the mineral. For an incoming parallel beam, two cases arise:

- (i) The surface of the mineral is flat (Figure 3a): all the rays follow similar paths entering the stone and then exiting it. They therefore remain parallel at the exit. If they are directed toward the observer, he sees a uniform sheen everywhere, otherwise the surface remains entirely dark.

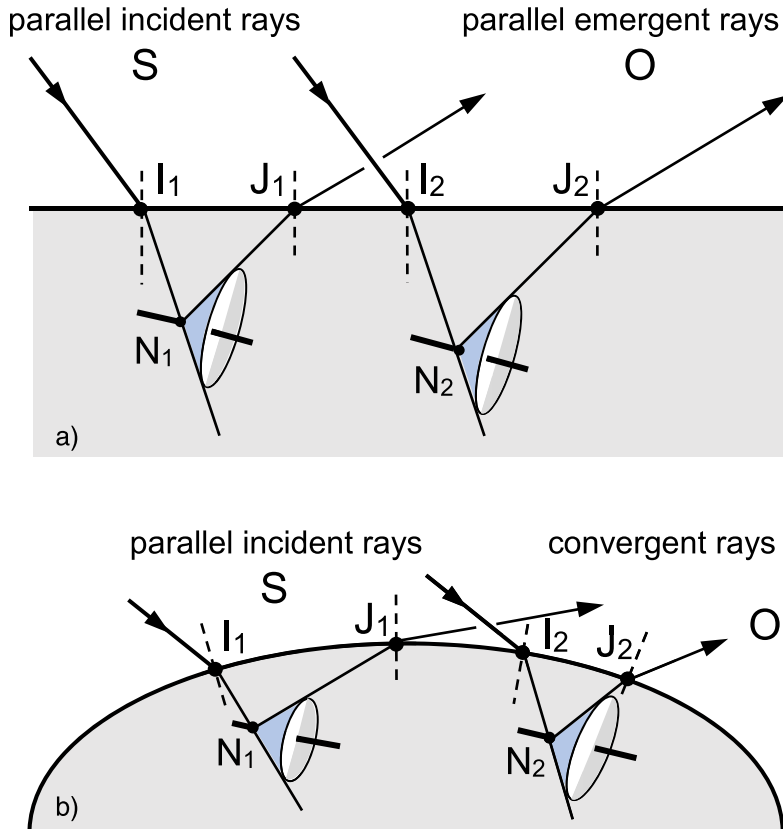


Figure 3. Illumination of the surface of a chatoyant stone with a parallel beam. Rays coming from a source S at infinity are refracted into the stone at I_1 and I_2 , reach the needles at N_1 and N_2 and are scattered as hollow cones. The rays of the cones located in the working plane emerge at J_1 and J_2 . The emergent rays are: (a) parallel in case of a flat surface: if they are in the direction of the observer O , also at infinity, all the surface is shining, creating a “sheen”; otherwise, the whole surface appears dark; (b) convergent in case of a curved surface: in this case, only one ray reaches the observer O , and the corresponding exit point J_2 indicates the position of the cat’s-eye.

- (ii) The surface is curved (Figure 3b): after entering the mineral, the rays are no longer parallel, neither in the stone, nor at their exit. A single ray reaches the observer and its exit point corresponds to the position of the cat’s-eye.

→ **This is why the gem has to be cut as a *cabochon*. In a stone with a curved surface, the observer will see a bright line, not a bright or dark surface.**

5. Mathematical approach

5.1. Overview of the problem

The general aim of the study is to follow the movement of the bright line characterizing the cat’s-eye phenomenon on the surface of a cabochon when the stone is rotated or when the observer or the source moves, and to determine the limits beyond which the phenomenon disappears.

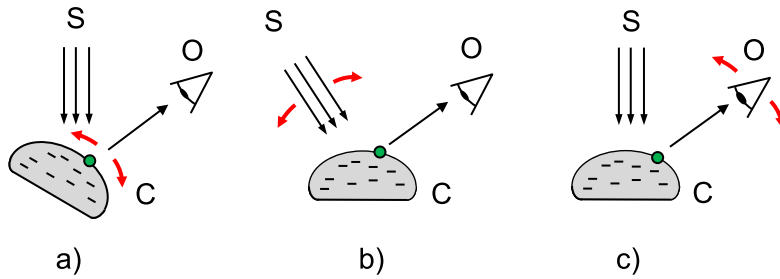


Figure 4. The sketch shows the three geometries for observing a cat's-eye: (a) the cabochon C rotates; (b) the lamp is rotated (angularly displaced) by the observer O ; (c) the observer moves in front of the cabochon. N.B.: (a) is the most frequent observation mode (S and O fixed); (b) often corresponds to a gemmological examination (C and O fixed). (c) is rarely used as an examination mode (S and C fixed).

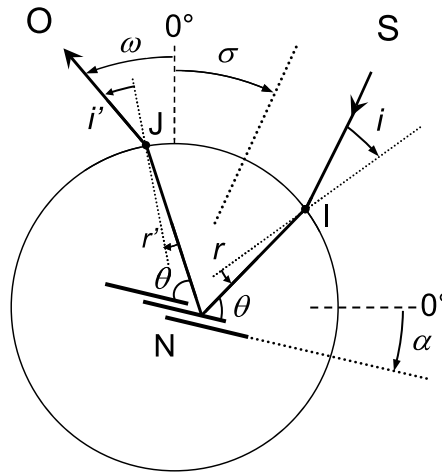


Figure 5. Angular parameters: Needle (N) tilt, α ; directions of source S , σ and observer O , ω ; entry and exit incidence angles i and i' ; α , σ , ω , i and i' are counted positively clockwise; refraction angles at the surface, r and r' (same sign as i and i' , respectively).

In the most common situation, the source is fixed (ceiling light or sun) and the observer sits or stands in front of his work table, and rotates the cabochon in his hand to look at the cat's-eye (Figure 4a). Less frequently, he moves a penlight over the static cabochon (Figure 4b). Rarely, he himself moves in front of the static cabochon illuminated by a ceiling light (Figure 4c).

In order to establish a general equation for these different cases, we define below the necessary parameters. We propose simplifying assumptions that are not too restrictive in order to facilitate the understanding and description of the phenomenon, and to develop a clear mathematical argumentation. We will then examine qualitatively what happens when these assumptions are not exactly satisfied.

6. Assumptions and definition of angular parameters (Figure 5)

6.1. Shape of the stone

We will first consider a cabochon of spherical shape to facilitate the mathematical analysis. Later, we'll consider the case of sharp or flat cabochons.

6.2. *Light source*

The light source S is located at infinity, so that the beam reaching the stone consists of parallel rays. Its angular position is defined by the angle σ , whose origin is counted from the vertical. The incidence angle i of a ray arriving on the sphere is defined from the direction of the source. This ray is refracted at the surface of the sphere at the angle r .

6.3. *Observer*

The observer O is also assumed to be at infinity so that he receives the rays from a specific direction, characterized by the angle ω . This is counted from the upper pole of the sphere.

6.4. *Needles*

Parallel acicular exsolutions are characterized by an azimuthal angle φ taken equal to zero (i.e. the needles are parallel to the working plane) and an angle α , counted from the horizontal plane. The incidence angle of a ray reaching a needle is denoted θ . This ray gives rise to a scattering cone with a half top angle θ . The main ray of this cone reaches the surface at a “refraction” angle r' and emerges into the air under the “incidence” angle i' .

N.B.: Angles i , i' , σ , ω and α are counted positively clockwise. For r and r' , which will appear by their trigonometric functions, it is worth mentioning that, according to the Snellius–Descartes law, their sign must be the same as that i and i' respectively, in calculations and drawings.

6.5. *Location of scattering elements*

Only needles located close to the surface will be considered. This is certainly true for nearly opaque stones such as cat’s-eye black diopside and star garnet, as well as most synthetic rubies and sapphires. Light that penetrates deeply into the stone is absorbed and only the rays scattered near the surface come out. In translucent gems, the light arriving on deeper needles has already been scattered once or several times by the needles near the surface [7]. The corresponding beams lose their intensity and coherence. Therefore, they contribute to the milky aspect and significantly less to the cat’s-eye. The proposed simplifying assumption is not unreasonable. It allows us to consider that the exit point J of an emerging ray is very close to the entry point I of the incident ray. $I (\approx J)$ is therefore the point at which the observer should aim. We can then equate the sphere with its tangent plane Σ at $I \approx J$ (see Figure 7).

6.6. *Angular restrictions*

(i) In order to consider all angular positions of the needles with respect to the light source, the angle α should in principle range from -90° to $+90^\circ$. However, the angular range over which the cat’s-eye can be observed is significantly reduced, due to the existence of a critical refraction angle.

(ii) The source can only illuminate half of the surface of the sphere and the observer can only receive rays from another half. If the directions of the source and the observer do not coincide, the rays reaching the observer come at most from a spherical section smaller than half of a sphere. In the plane of Figure 6, the possible angular positions of point $I \approx J$ range from $\omega - 90^\circ$ to $\sigma + 90^\circ$, which means over $180 - (\omega - \sigma)$ degrees.

→ **The angular range of visibility of the cat’s-eye decreases as the direction of observation moves away from that of the source. When the source and the observer are oriented in the same direction, the cat’s-eye is seen in the widest angular range.**

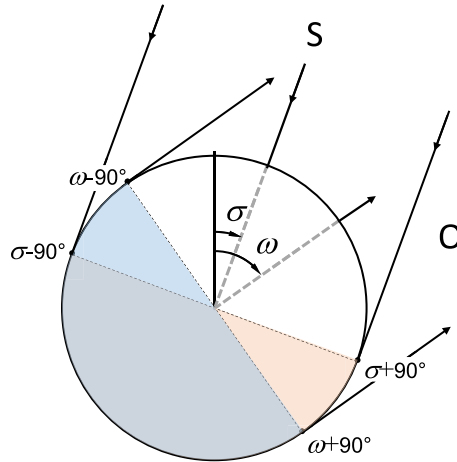


Figure 6. Restricted domain of visibility of the cat's-eye when the directions of the source S and the observer O do not coincide.

6.7. Refractive index of the material

An incident ray at angle i is refracted at angle r , in accordance with the Snellius–Descartes law: $\sin i = n \cdot \sin r$ (where n is the refractive index). A ray scattered by a needle emerges in the air according to the same law, $\sin i' = n \cdot \sin r'$, with a limit value for $i_{\text{lim}} = i'_{\text{lim}} = 90^\circ$ and a corresponding critical refraction angle $r_{\text{lim}} = r'_{\text{lim}} = \arcsin(1/n)$. The impact of the refractive index will be studied later in the case of four chatoyant minerals.

7. Needles in the main plane

We consider here the great circle of the sphere, coplanar to the directions of the source and the observer, and we assume that the needles are parallel to this plane. It constitutes a plane of symmetry for the scattering cones surrounding the needles it contains. This plane intersects two specific rays of the cone, one being an extension of the incident ray on the needle (IN). Earlier described as the **main ray**, the other (NJ) is located in the main plane, even after refraction in the air at point $J \approx I$ (I, J, N illustrated on Figure 3b). Only this point of the cat's-eye will be mathematically defined, but it will govern the whole movement of the bright band of chatoyancy.

We will follow the evolution of this point J when the sphere, and thus the needles, rotate around an axis perpendicular to the main plane. In our assumptions, since the needle is just below to the surface, points J and I are close to each other on plane Σ , tangent to the sphere, as explained earlier. We therefore study the position of point $J (\approx I)$ at which the emergent ray points toward the observer. It is characterized by the angle i between the incident ray and the normal to the plane tangent to the sphere at point I , as a function of the needle orientation, α . This angle i is the unknown which corresponds to the angular position $\sigma - i$ of the cat's-eye apex on the sphere. It must be evaluated as a function of parameters α , σ , and ω (Figure 7).

8. Determination of the angular position $\sigma - i$ of the cat's-eye

Figure 7 represents the path followed by a ray from the source to the observer, first refracted at point I , arriving on the needle at point N under angle θ , then scattered on the needle under the same angle θ , giving rise to the **main ray** NJ , refracted and emerging at point J . All angles

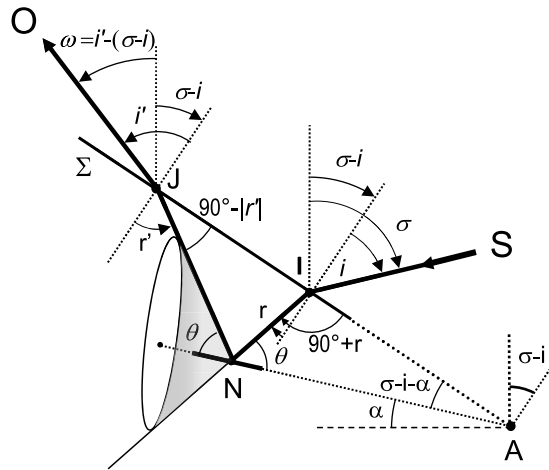


Figure 7. Optical path of a ray emanating from the source *S*, refracted at point *I*, scattered by a needle at point *N* under angle θ . The main ray scattered under the angle θ is refracted at point *J* to emerge in the direction of the observer *O*. The respective angular directions σ and ω of the source and the observer are defined with respect to the vertical, the tilt angle α of the needles with respect to the horizontal, and the angles of incidence and refraction i , i' , r and r' with respect to the normal to the tangent plane Σ of the sphere at points *I* or *J*. Angles α , σ , ω , i and i' are counted positively clockwise; r and r' must be of the same sign as i and i' , respectively (thus, the angle $NIJ = 90^\circ - |r'| = 90^\circ + r'$, where r' is negative with an absolute value equal to $|r'|$). With the initial simplifying assumptions, the point $I \approx J$ corresponds to the top of the bright line representing the cat's-eye at the surface of the spherical cabochon, at the angular position $\sigma - i$. Σ is the trace of the tangent plane to the sphere at point $I \approx J$.

defined previously are depicted in Figure 7. With the extension of the directions of the needle and the trace of the tangent plane Σ to the sphere, we can establish angular relations from:

triangle *NIA*: $180 = (90 + r) + \theta + (\sigma - i - \alpha)$.

triangle *NJA*: $180 = (90 + r') + (180 - \theta) + (\sigma - i - \alpha)$.

Which express that the sum of the angles in a triangle is equal to 180°. Eliminating θ between these two formulae, we obtain:

$$\sigma - i = \alpha - (r + r')/2 \tag{1}$$

or (with $\omega - i' = \sigma - i$: see angles near point *J*)

$$i' = i + \omega - \sigma. \tag{2}$$

These simple equations govern the position of the point of emergence $J \approx I$ and therefore the angular position $\sigma - i$ of the cat's-eye. The purpose of the following mathematical operations is only to express r , r' and i' as a function of i , using the Snellius–Descartes law, which is written as follows:

$$\sin r = \sin i/n \quad \text{or} \quad r = \arcsin(\sin i/n) \quad \text{and similarly, } r' = \arcsin(\sin i'/n).$$

Replacing now r , r' and i' versus i in Equations (1) and (2), we get:

$$\sigma - i = \alpha - \{\arcsin[\sin i/n] + \arcsin[\sin(i + \omega - \sigma)/n]\}/2. \tag{3}$$

Equation (3) is the form of Equation (1) which derives from the simple Snellius–Descartes law applied to the light ray coming in and out of the spherical sample surface, allowing to

operate practical calculations. Such trigonometric equation (earlier called “transcendental”) can be solved by considering each of the terms on either side of the sign equal as a function y or y' :

$$y = \sigma - i$$

$$y' = \alpha - \{\arcsin[\sin i/n] + \arcsin[\sin(i + \omega - \sigma)/n]\}/2. \quad (4)$$

The graphical solution of Equations (4) is given by the intersection of the straight-line y and the curve y' .

Examples are provided in the following paragraphs. The curves are obtained from tables of values calculated for y and y' . The range of application of these curves is limited by the values defined in the previous paragraph 6.6 “angular restrictions”.

9. Determination of the relative movement of the cat’s-eye

The pair of Equations (4) will be used to follow the displacement of the cat’s-eye as one of the three entities moves (source, observer or needles), the other two being fixed. To highlight the direction of motion, we will write Equation (3) for two values of the variable parameter, setting an arbitrary value to the other two parameters. As example, sillimanite will be considered for practical calculations, with its refractive index $n = 1.66$.

9.1. Rotation of the stone: α (needles) variable, ω and σ (source and eye) fixed

We take for example $\sigma = 20^\circ$ and $\omega = -30^\circ$, and solve Equations (4) for $\alpha = -15^\circ$ and $\alpha = +15^\circ$. The graphical resolution is presented in Figure 8a. The straight line y does not depend on α , and thus is the same for both values of α . The two curves $y' = \alpha - \arcsin[\sin i/n]$ are similar, only offset vertically by 30° , when passing from $\alpha = -15^\circ$ to $\alpha = +15^\circ$. The approximate solutions correspond to $i \sim 47^\circ$ and $i \sim -16^\circ$ (orange and blue vertical arrow, respectively). A refinement carried out with a step of 0.1° on the horizontal axis gives more accurate values (47.45° and -16.84°), obtained from the insets in Figure 8a. Thus, the angular position of the cat’s-eye moves from $\sigma - i = -27.45^\circ$ to $\sigma - i = 36.84^\circ$, corresponding to a displacement of 64.29° (orange and blue horizontal arrows, respectively), while the needle tilt angle α increases as well, from 30° (Figure 8b). The following can be concluded:

→ **When the stone rotates in one direction, the observer and the source being fixed, the cat’s-eye moves faster, in the same direction.**

9.2. Movement of the source: σ variable, α and ω (needle and observer) fixed

This time, we assign simple values to the needle tilt and the observer angle, for instance: $\alpha = 0^\circ$ and $\omega = 0^\circ$. In these conditions, the range of validity for the point $I \approx J$ extends from -90° to $+90^\circ$.

Let us take two values of the source direction: $\sigma = 0^\circ$ and $\sigma = 30^\circ$.

For $\sigma = 0^\circ$, Equation (3) is easily solved: $i = \arcsin(\sin i/1.66)$, verified if, and only if, $i = 0$. Thus, $\sigma - i = 0$, and point $I \approx J$ stays at the apex of the great circle.

For $\sigma = 30^\circ$, the Equations (4) become:

$$y = 30^\circ - i \quad \text{and} \quad y' = \{\arcsin(\sin i/1.66) + \arcsin[\sin(i - 30^\circ)/1.66]\}/2.$$

In Figure 9a, the graphical solution is located at the intersection of the straight line y (in black) and the curve y' (in blue). In the inset of the same figure, a refinement of the measure gives the value: $\sigma - i = -19.36^\circ$. The whole light path from the source to the observer is plotted in blue on Figure 9b.

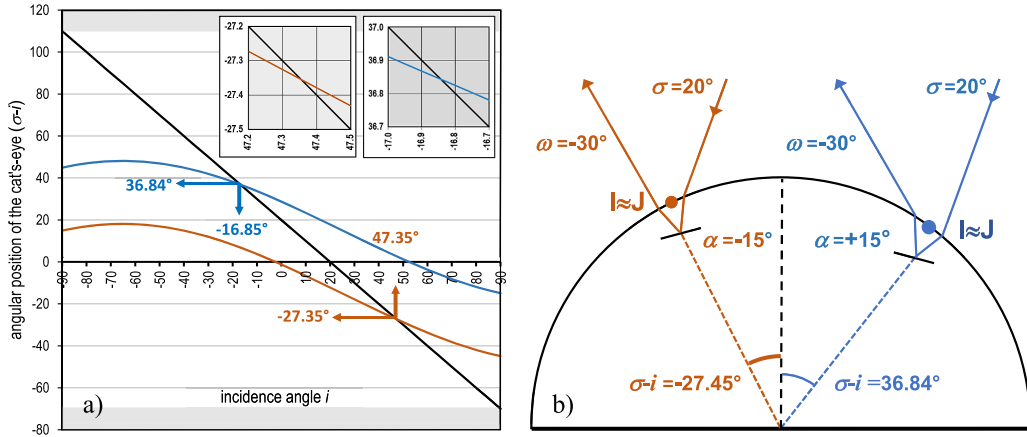


Figure 8. (a) Practical example of graphical solution for the case of sillimanite ($n = 1.66$), where Equations (4) are plotted as a function of angle i in order to obtain the angular positions $\sigma - i$ of the cat's-eye apex with a light source located in the direction $\sigma = 20^\circ$ and an observer at $\omega = -30^\circ$, for needle tilt angles $\alpha = \pm 15^\circ$. The solutions (orange and blue arrows) lie at the intersection points between the straight-line y (in black) and the curves y' (orange for $\alpha = -15^\circ$ and blue for $\alpha = +15^\circ$). The line y remains unchanged, while the curves y' shift by 30° , corresponding to the change from $\alpha = -15^\circ$ to $\alpha = +15^\circ$. (b) Optical paths for these two situations: When α increases by 30° , the angular position $\sigma - i$ of the cat's-eye also increases by 64.29° (from the orange point to the blue point $I \approx J$).

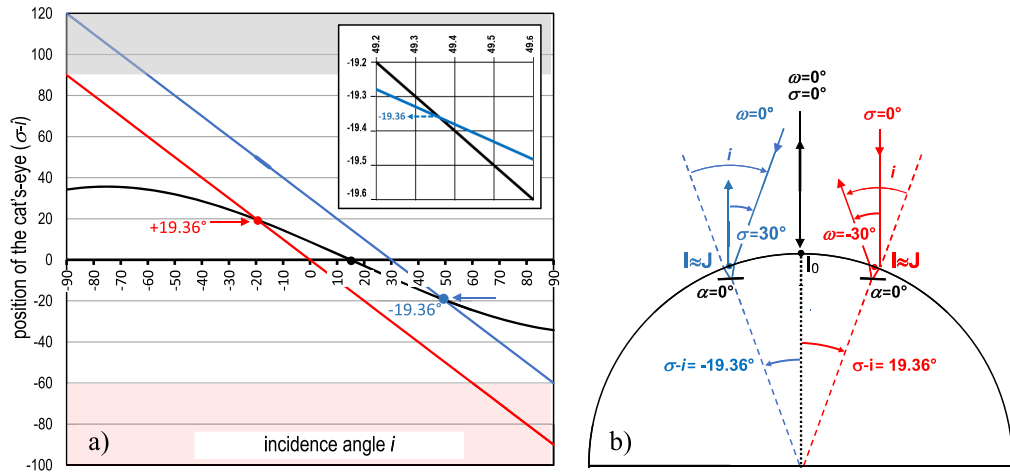


Figure 9. (a) Solving the equations giving the angular position of the cat's-eye when the source or the observer moves. We fix the needle tilt equal to 0° , as well as the initial values of σ and ω , corresponding to the black point on the horizontal axis. Then, we successively change the value of σ ($= 30^\circ$) or the value of ω ($= -30^\circ$). For each value of σ or ω , curve y' is identical in both cases (in black). In the former case, the angular position $\sigma - i$ is negative, and positive in the latter. (b) Representation of the light paths in both cases. The cat's-eye, initially represented by point I_0 , moves in the opposite direction of the source (from black point I_0 to blue point I) or of the observer (from black point I_0 to red point I).

Thus, from $\sigma = 0^\circ$ to $\sigma = 30^\circ$, the angle $\sigma - i$ associated with the point I changes from 0° to -19.36° which means the following:

→ **When the lamp angularly moves away from the observer, with the latter and the stone fixed, the cat's-eye rotates more slowly, in the opposite direction.**

9.3. Movement of the observer: ω variable, σ and α (gem and source) fixed

Taking the simple values $\sigma = 0^\circ$ and $\alpha = 0^\circ$, we now choose two values of ω (0° and -30°):

For $\omega = 0^\circ$, Equation (3) is again $i = \arcsin(\sin i / 1.66)$, verified if, and only if, $i = 0^\circ$ and the cat's-eye remains at the apex of the spherical cabochon.

For $\omega = -30^\circ$, the Equations (4) are expressed as:

$$y = i \quad \text{and} \quad y' = \{\arcsin(\sin i / 1.66) + \arcsin[\sin(i - 30^\circ) / 1.66]\} / 2.$$

Compared to the previous case, $y = \sigma - i = -i$ is a straight line, parallel to the previous one, but shifted downwards by 30° , and y' is formally identical, represented by the same curve (in black) in Figure 9a. In Figure 9b, the light path is drawn in red. It appears symmetrical with respect to the median vertical plane, with an inversion of the direction of light propagation. The position of point $I \approx J$ is also inverted, with the value of $\sigma - i = 19.36^\circ$, opposite to that in the previous paragraph.

Thus, when the observer moves from $\omega = 0^\circ$ to $\omega = -30^\circ$, point $I \approx J$ slips angularly from $\sigma - i = 0^\circ$ to $\sigma - i = 19.36^\circ$, which implies the following:

→ **When the observer moves in one direction, the stone and the source being fixed, the cat's-eye moves more slowly, in the opposite direction.**

9.4. Angular ranges for observing the cat's-eye, with a source at vertical and an observer at any angle ω

By rotating the sphere around an axis perpendicular to the working plane (which contains the needles regardless of their tilt angle α), in which angular range ω will an observer distinguish the cat's-eye? This question is not uninteresting because the light source is not always located above the gem; it can be placed at a different angle on a table or a desk, and the observer is therefore not necessarily in the same direction as the source. And even if the source is above the gem, the observer being placed next to the stone can, without moving, raise it towards the lamp, and thus the source and the observer are no longer in the same direction. To answer this question, we must express α versus $\sigma - i$ for different values of ω . Using again the refractive index of sillimanite and a source at $\sigma = 0^\circ$, Equation (3) is inferred as follows:

$$\alpha = -i + \{\arcsin[\sin i / 1.66] + \arcsin[\sin(i + \omega) / 1.66]\} / 2. \quad (5)$$

This function is plotted versus $\sigma - i = -i$ on Figure 10a for the following values of ω : 0° , 20° , 40° , 60° , 80° , 100° , 120° , 140° , 160° , 180° .

These curves show that for a given value of ω , the angular range $\sigma - i = -i$ (with $\sigma = 0^\circ$) decreases when the observer moves angularly away from the source.

→ **When the cabochon rotates under a ceiling lamp, the range of visibility of the cat's-eye narrows as the observer moves angularly away from the vertical.**

N.B.: If the observer only moves the cabochon progressively upwards without rotating the stone, the observation time of the cat's-eye varies depending on the tilt angle α . The widest range of variation of ω , and therefore of the visibility of the cat's-eye, indicated by the black arrows, lies between the values associated with the violet ($\omega = 0^\circ$) and green ($\omega = 100^\circ$) curves. It corresponds to an α value of about 28° . The cat's-eye will not be at the apex of the cabochon, but will evolve between the angular positions 10° and 60° approximately (vertical dotted lines).

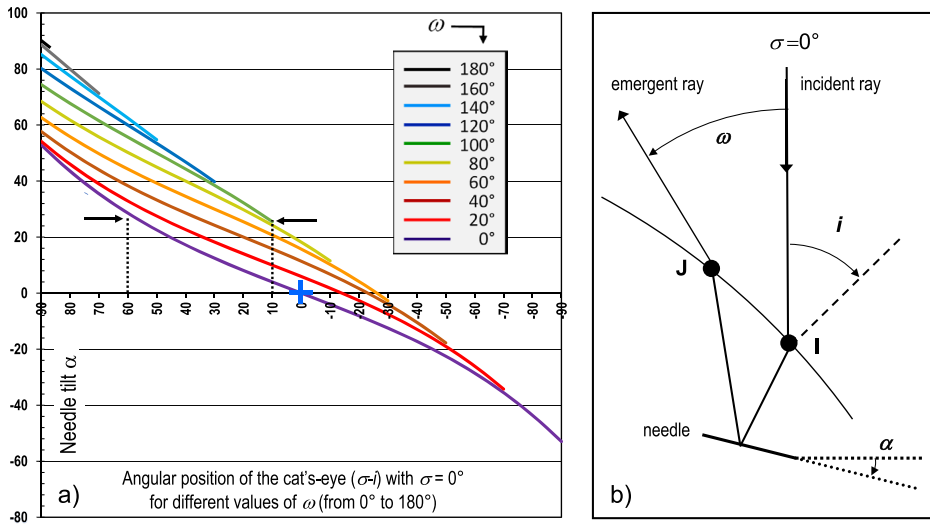


Figure 10. (a) Curves α versus $\sigma - i$ showing the ranges for which the cat’s-eye is visible, for a vertically oriented source and for an observer looking at different directions ω , from 0° to 180°. The more this angle increases, the more the observation of a cat’s-eye is reduced, as demonstrated by increasingly smaller curves. The blue cross corresponds to the most pleasant situation with a central position of the cat’s-eye ($\sigma - i = 0^\circ$ with $\alpha = 0^\circ$, $\sigma = 0^\circ$, $\omega = 0^\circ$). The horizontal black arrows indicate an approximate value of the needle inclination α (about 28°) for which the angular variation of the observation $\Delta\omega$ is the largest (from 0° to 100°), corresponding to an angular variation $\Delta(-i)$ of the cat’s-eye (from 60° to 10°), when the stone is translated upwards. (b) Diagram of the light path for $\sigma = 0^\circ$ with α and ω variable.

9.5. Influence of the refractive index

It is interesting to assess the angular range of α for which the cat’s-eye is visible depending on the refractive indices, from low to high values. We operate in classical and optimal conditions ($\sigma = 0^\circ$ and $\omega = 0^\circ$), for which Equation (3) becomes:

$$\alpha = -i + \arcsin[\sin i / n] = h(i).$$

We consider the cases of four chatoyant minerals: opal, sillimanite, garnet and the rare cat’s-eye rutile [8] with refractive indices around 1.43, 1.66, 1.80 and 2.7 respectively. Figure 11 shows the curves α versus i for these four indices. The maximal angles α deduced from the graph are about $\pm 45^\circ$, $\pm 53^\circ$, $\pm 56^\circ$ and $\pm 68^\circ$. This means that there is a substantial difference in the overall observation ranges $\Delta\alpha$ of the cat’s-eyes between the two extreme cases: 90° for opal (blue double arrow) and 136° for rutile (orange double arrow). In each case, under the same chosen conditions ($\sigma = 0^\circ$ and $\omega = 0^\circ$), the incidence angle i changes from -90° to $+90^\circ$ and the position of the cat’s-eye moves from 90° to -90° . But at the same time, the angles of rotation of the stone are very different. For the observer, it is more comfortable to watch the cat’s-eye over a larger range of stone rotation (case of rutile).

→ **The angular range of visibility of the cat’s-eye when the cabochon rotate increases with the refractive index. In other words, for an identical rotational velocity of the cabochon, the higher the refractive index is, the longer the observer is able to watch the cat’s-eye.**

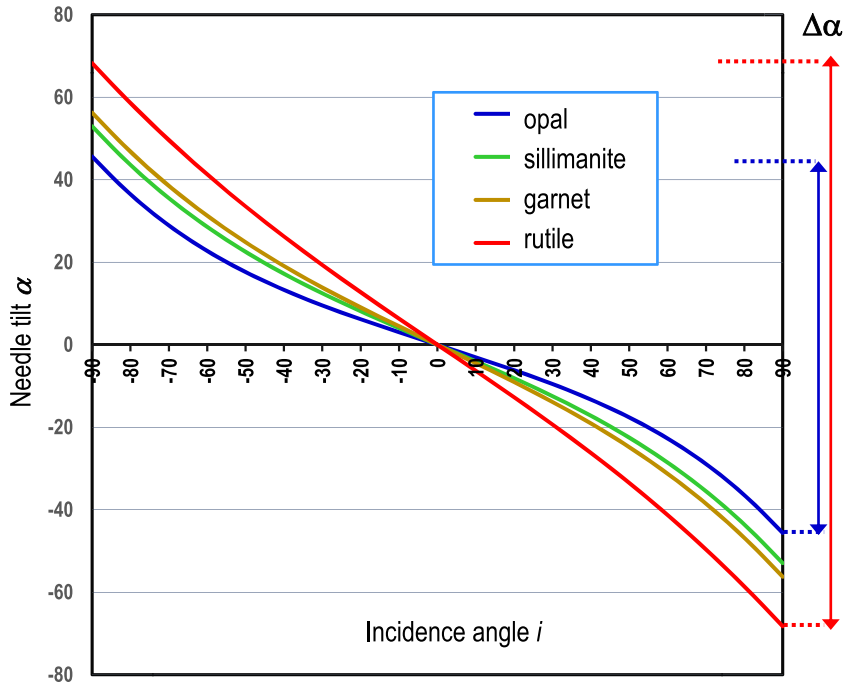


Figure 11. $\alpha = h(i)$ curves for different refractive index values in chatoyant or asteriated gems. $\Delta\alpha$ values are 90° for opal (blue arrow) and 136° for rutile (red arrow).

10. Illustration of the three modes of observation: the practical example of sillimanite

To illustrate the results inferred from the mathematical development, we chose an oval cabochon of sillimanite (approximately $23.5 \times 20.8 \times 11.2$ mm; mass 46.81 ct) originating from India. It has a dark greenish-gray color, and its refractive index is 1.66, measured at the base of the cabochon. It belongs to the collection of Pascal Entremont. We photographed the stone for five angular values of a varying parameter σ , ω or α , the other two being fixed at zero: 0° , 15° , 30° , 45° and 60° . Let us consider the three configurations (note that the case where all parameters are equal to 0° belongs to each series of photographs), as illustrated in Figure 12.

10.1. *Rotation of the stone with $\sigma = 0^\circ$ and $\omega = 0^\circ$ (source and observer directly above the cab)*

The cat's-eye rotates in the same direction as the cabochon does (Figure 12, bottom series). It should be noted that this type of observation is the most common and the most convenient, and definitely the most instinctive. The observer, placed under a lamp above him (preferably a point light source), holds the stone low enough against him, and turns it slowly in one direction or another, the cat's-eye moving around a horizontal rotation axis. The observation angle ω is low and thus the limitation of the field of view ($\pi - \omega$) is reduced to a minimum. The cat's-eye remains sharper compared to the other cases, even for large angles, but the most pleasant situation corresponds to a symmetrically positioned cat's-eye, when all parameters are equal to 0° (Figure 12, center left).

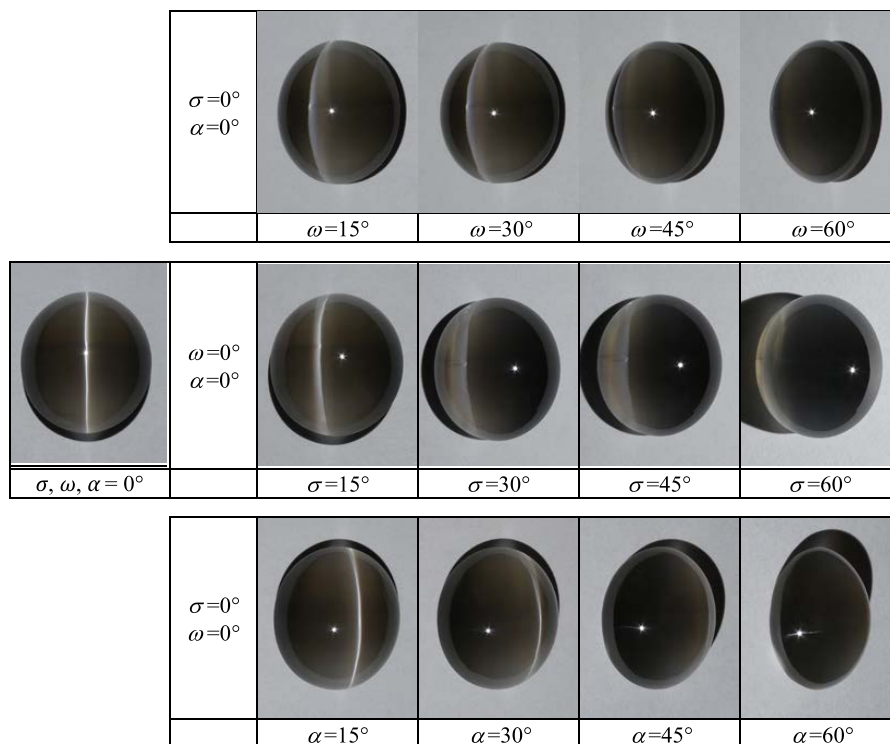


Figure 12. Photographs of the cat's-eye positions for three configurations, with one varying parameter: ω (top; angle of the observer away from the normal to the cab), σ (middle: angle of the source with the normal) or α (bottom; needle tilt). The sharpest line corresponds to the third case, where α varies, σ and ω are set to 0° . This is also the most natural and comfortable observation condition. However, the most pleasant situation occurs when all angles are equal to 0° (left). At high values of α , σ or ω , the cat's-eye disappears. The stone was illuminated by a white point light source at a distance of about 30 cm and the needles producing the cat's-eye are parallel to one of the optic axes of this sillimanite [9]. P. Entremont's collection. Photos by Thanh Nhan Bui.

10.2. Motion of the lamp, with $\alpha = 0^\circ$ and $\omega = 0^\circ$

The cat's-eye rotates in the opposite direction to the lamp. Handling is easy for the observer, especially with a penlight. But the cat's-eye quickly becomes diffuse as σ increases (Figure 12, middle series). Since the current sample of sillimanite is not totally opaque, the "coffee and cream" effect appears (see additional considerations, Section 11.2).

10.3. Motion of the observer with $\sigma = 0^\circ$ and $\alpha = 0^\circ$

Actually, the observer does not physically move, but he gradually raises the stone toward the source without changing its orientation. This option is the less convenient for him. Therefore, ω varies and the cat's-eye rotates in the opposite direction as the observer. Moreover, when ω increases, the cat's-eye becomes diffuse and the "coffee and cream" effect also appears (Figure 12, top series).

Finally, the experimental cat's-eye behavior, as observed in the case of sillimanite (Figure 12), is in full agreement with the predicted theory when the angular parameters α , σ or ω vary.

11. Comments on the preliminary assumptions and additional considerations

11.1. *Source and observer at infinity*

We assumed that the source is reduced to a point located at infinity. The sun suits this assumption quite well (apparent diameter: $\sim 0.5^\circ$) and allows the observation of a sharp cat's-eye. A close and large source provides a convergent beam, so that there are various rays emerging towards the observer, causing the cat's-eye to widen. With respect to the observer, the apparent pupil diameter of his eyes ($\sim 1^\circ$) is not sufficient to cause a noticeable widening of the cat's-eye.

Conventional desk lamps give a wider and less convincing light strip. Diffuse ceiling light, "neon tubes", multiple LEDs, or cloudy daylight are too large a source and are not suitable for observing the cat's-eye phenomenon correctly.

11.2. *Scattering by deep needles within the stone*

Depending on the translucency of the mineral, deep needles can contribute to the creation of a cat's-eye. In such cases, the emergence point J will no longer coincide with the incidence point I , and will depend on the position of each deep needle. This can lead to an enlargement of the cat's-eye. Moreover, under oblique lighting, an asymmetrical effect, named "milk and honey" in yellow gems such as chrysoberyl [10], Liddicoat [11] or "coffee-and-cream" in brown gems, appears in translucent cabochons and consists of two distinct areas on both sides of the cat's-eye: a dark one on the side of the light source and a bright one on the opposite side. These contrasting areas are due to deep acicular inclusions within the stone that illuminate one side of the cabochon, as clearly explained by Killingback [12].

Note that when $\sigma = 0^\circ$ and $\omega = 0$, Equation (2) is reduced to $i' = i$ and therefore $r' = r$. This requires the main scattered ray to coincide with the incident refracted ray. Then, both rays must be perpendicular to the acicular inclusions (Figure 13). It follows that, regardless of the inclination α of the needles, the path of both incident and emergent light rays is identical. This means that the entry and exit points I and J are no longer close to each other (as it was the case for needles close to the surface), but they strictly coincide, whatever their depth. We can therefore expect a very sharp cat's-eye, without any "coffee and cream" effect, even at large α angles (Figure 12, bottom series).

11.3. *Shape of the cabochon*

For the sake of simplified calculations, we considered a spherical cabochon. In fact, most cabochons display a semi-elliptical or semi-ovoid cross-section, which is approximately modeled by two different radii (R and R') of curvatures ($1/R$ and $1/R'$),—one at the apex, the other at the edges—, leading to two types of shapes: flat and sharp cabochons.

The cross-section of these two types of cabochon was drawn for a ratio $R'/R = 2.5$ between the central and lateral curvatures, with an inversion of the radii between Figures 14a (flat cabochon) and 14b (sharp cabochon). When the stone is rotated through a given angle (in pink), the cat's-eye travels a distance 2.5 times greater for the small $1/R'$ curvature than for the larger $1/R$ curvature (Figure 14c). In the case of a flat cabochon, the cat's-eye will move much more spatially around the apex ($\times 2.5$) than in the case of a sharp cabochon.

On the other hand, while cat's-eyes may widen due to a convergent beam of light or to some stone transparency, they still remain narrower on sharp cabochons than on flat cabochons.

→ **When the stone is rotated, the mobility of the cat's-eye is better experienced on flat cabochons than on sharp cabochons. However, narrower cat's-eyes are expected on sharp cabochons.**

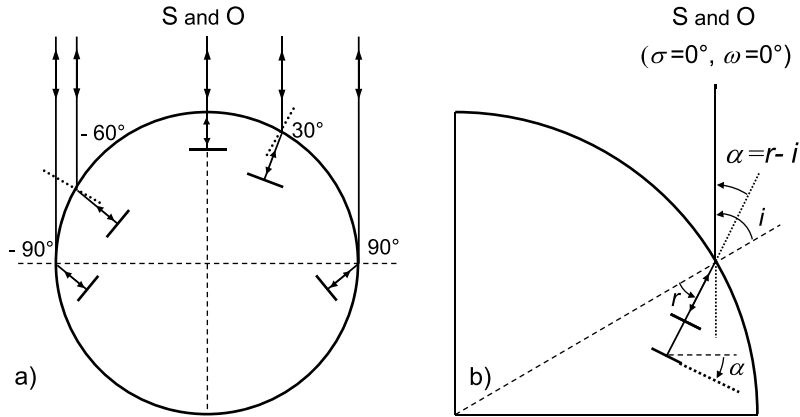


Figure 13. Source and observer in the same vertical direction ($\sigma = 0^\circ$ and $\omega = 0^\circ$): (a) The main scattered ray follows the same path as the incident ray, both perpendicular to the needles and the behavior of the cat’s-eye is symmetrical with respect to the vertical plane passing through the center of the sphere and perpendicular to the working plane when the angle ranges from -90° to $+90^\circ$. (b) Details of angular parameters.

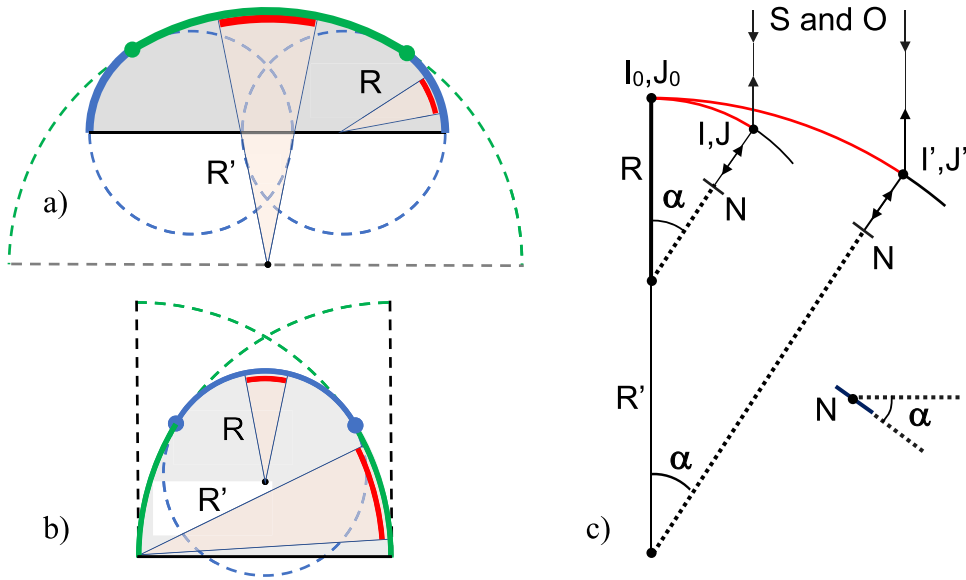


Figure 14. Modeling an ovoid cabochon using a central circle and two side circles: (a) flat cabochon; (b) sharp cabochon. (c) For a source and an observer oriented vertically, with a needle (N) tilt varying from 0° to α , the cat’s-eye moves away from the upper pole of the sphere of radius R or R' by a distance $\alpha \cdot R$ or $\alpha \cdot R'$, respectively. The ratio R'/R is taken as 2.5.

11.4. *Needles perpendicular to the main plane, with arbitrary σ and ω*

This case corresponds to the azimuth angle $\varphi = 90^\circ$, where needles are perpendicular to the main plane (Figure 15). Needle portions located in the main plane containing the source and observer directions scatter light into flat cones with centrifugal rays. Regardless of the entry points I in this plane, there is always an emergent ray from the great circle towards the observer. This is the only

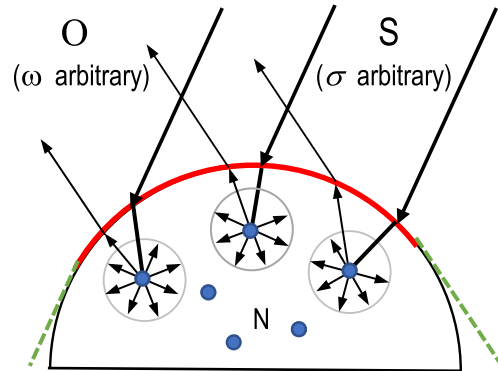


Figure 15. As the needles N are perpendicular to the drawing plane, the scattering cones are flat (half top angle equal to 90°). Emerging rays, located in the main plane, propagate in all observation directions belonging to this plane. The dotted lines in green, tangent to the sphere and parallel to the directions of the source S and the observer O , delimit the cat's-eye (in red) according to the angular restrictions mentioned in Section 6.6.

case where we can easily describe the exact position of the entire cat-eye line without further calculation. Note also that it is no longer necessary to assume that the needles are close to the surface. On the other hand, needle portions outside the main plane give rise to scattering cones with a half top angle below 90° . The rays thus emerge laterally and cannot reach the observer.

The cat's-eye is therefore a bright line on the great circle (in red), in the main plane. However, its extension is limited by the angular values of σ and ω , according to the restrictive conditions indicated in paragraph 6.6.

→ **When needles are perpendicular to the directions of both the source and the observer, a bright line settles on a great circle in the main plane. This applies for any position of the sphere rotating around the needle axis.**

11.5. *Wavy parallel fibers*

When a bundle of parallel fibers progressively changes direction, following a wavy pattern in a crystalline matrix with a polished flat surface, the chatoyancy will not appear everywhere for the same position of the source and the observer as in Figure 3a. There will be bright and dark areas, moving very quickly as the stone is gradually tilted, giving moiré patterns. This is the case for tiger's-eye, hawk's-eye or iron-eye quartz which present an undulating chatoyancy. Also included are serpentine, chatoyant clinoclure (seraphinite), as well as charoite.

11.6. *Roughly oriented needles along a mean direction*

When needles, such as microfibers, are not arranged in a strict crystallographic orientation in the host crystal, but are slightly disoriented along an average axis, they do not induce a sharp cat's-eye on a cabochon, but display a wide band of chatoyancy. This can be observed for instance in quartz microfibers in chalcedony [13].

11.7. *Binocular vision*

The observer's eyes are two slightly separate receptors, so he should see two separate cat's-eyes on the stone, but very close to each other. However, the brain superimposes and merges the two

images to create a single image over the cabochon. This is the stereoscopic effect, as described by Killingback [12] and supplemented by Bui *et al.* [14], which is beyond the scope of the present paper.

12. Conclusion

We limited the mathematical description of a cat's-eye to the search for the position of the light spot generated by a specific ray of a light beam scattered by parallel needles embedded in a mineral matrix cut *en cabochon*, which we called "the main ray". The study of the exact location of all points of the cat's-eye line is beyond the present work. Nonetheless, the angular behavior of the source, observer, and stone was successfully established through a straightforward trigonometric formalism, using only the so-called Snellius–Descartes law, thanks to a number of relevant assumptions.

This well-defined approach allows us to understand and justify the already experimentally known qualitative behavior of the cat's-eye moving on the surface of cabochons for three modes of observation. The motion of the cat's-eye, as intuitively perceived by the observer, is in full agreement with our mathematical development.

Declaration of interests

The authors do not work for, advise, own shares in, or receive funds from any organization that could benefit from this article, and have declared no affiliations other than their research organizations.

Acknowledgment

The authors are indebted to Professor Emmanuel Fritsch (University of Nantes, France) for his invaluable advice and contribution to the revision of the manuscript.

References

- [1] M. P. Steinbach, *Asterism – Gems With a Star*, Odd GmbH & Co. KG: Bad Kreuznach, 2016, p. 896.
- [2] A. Wüthrich and M. Weibel, "Optical theory of asterism", *Phys. Chem. Miner.* **7** (1981), no. 1, pp. 53–54.
- [3] M. Weibel, "How is the star formed? Asterism and chatoyancy in gemstones", *Lapis* **7** (1982), no. 10, pp. 25–27. 30, 38.
- [4] E. J. Gübelin, M. Weibel and A. Wüthrich, "Elucidating the optical theory of asterism", *J. Gemmol. Soc. Japan* **9** (1982), no. 1, pp. 18–21.
- [5] A. Wüthrich, M. Weibel and E. J. Gübelin, "Elucidating the optical theory of chatoyancy and asterism", *Austr. Gemmol.* **15** (1983), no. 1, pp. 3–5.
- [6] S. Yokoi, K. Kurashige and J. I. Toriwaki, "Rendering gems with asterism or chatoyancy", *Visual Comput.* **2** (1986), no. 5, pp. 307–312.
- [7] H. Killingback, "Stereoscopic effect in asterism and chatoyancy", *J. Gemmol.* **29** (2005), no. 5–6, pp. 312–315.
- [8] C. W. Fryer, "Cat's-eye rutile", *Gems Gemol.* **22** (1986), no. 2, p. 111.
- [9] M. E. Fleet and M. Arima, "Oriented hematite inclusions in sillimanite", *Am. Mineral.* **70** (1985), no. 11–12, pp. 1232–1237.
- [10] R. Crowningshield, "Yellow cat's-eye apatite", *Gems Gemol.* **11** (1963), no. 2, p. 44.
- [11] R. T. Liddicoat Jr, "Glass cat's-eye", *Gems Gemol.* **14** (1972), no. 4, p. 108.
- [12] H. Killingback, "The 'coffee-and-cream' effect in chatoyant cabochons", *J. Gemmol.* **34** (2015), no. 6, pp. 524–530.
- [13] J. P. Gauthier and J. Fereire, "Chatoyancy of chalcedony", *Revue Gemmol. AFG* **218** (2022), pp. 7–9. in French.
- [14] T. N. Bui, P. Entremont, F. Mazzero and J. P. Gauthier, "Stereoscopy in asteriated gemstones revisited", *J. Gemmol.* **37** (2020), no. 3, pp. 298–305.